

Optimized Finite-Time Work Protocols for the Higgs RNA-Model

Peter Werner* and Alexander K. Hartmann†

Institut für Physik, Universität Oldenburg, 26111 Oldenburg, Germany

(Dated: October 6, 2023)

The Higgs RNA-Model [1] is studied in regard to finite-time driving protocols with minimal-work requirement. In this paper, RNA sequences which at low temperature exhibits hairpins are considered, which are often cited as typical template systems in stochastic thermodynamics. The optimized work protocols for this glassy many-particle system are determined numerically using the parallel tempering method. The protocols show distinct jumps at the beginning and end, which have been observed previously already for single-particle systems [2–4]. Counter intuitively, optimality seems to be achieved by staying close to the equilibrium unfolding transition point. The change of work distributions, compared to those resulting from a naive linear driving protocol, are discussed generally and in terms of free energy estimation as well as the effect of optimized protocols on rare work process starting conditions.

I. INTRODUCTION

Moving a system from an initial state at time t_0 to some final state at t_f by varying an external control parameter $\lambda(t)$ in a finite period of time $t \in [0, \tau]$ requires an amount of work $W[\lambda(t)]$ that is in general a functional of the driving. In classical thermodynamics for macroscopic systems, a lower bound for the required work is given by the difference in free energy ΔF between the equilibrium states at the initial and final control parameters

$$W[\lambda(t)] \geq \Delta F \equiv F(\lambda(\tau)) - F(\lambda(0)), \quad (1)$$

where equality holds for quasi-static, infinitely slow driving (i.e. $\tau \rightarrow \infty$). For mesoscopic systems, thermal fluctuations are a relevant contribution to the path the system takes when subjected to the driving protocol $\lambda(t)$. Hence, the work W is not a simple scalar value anymore but a stochastic quantity that fluctuates each time the work process is repeated and therefore follows a distribution $P_\lambda(W)$. Note that the distribution for small systems often have significant contributions even for $W < \Delta F$, i.e., energy might be taken from the bath. These work distributions and their moments usually fulfill various relations, like Crook's theorem [5] or the Jarzynski equality [6]

$$\langle e^{-\beta W} \rangle = e^{-\beta \Delta F}, \quad (2)$$

with the inverse temperature $\beta = \frac{1}{k_B T}$, where the scale $k_B = 1$ is used in the following. The average $\langle \dots \rangle$ is over the initial equilibrium at $\lambda = \lambda(0)$ and all non-equilibrium trajectories $\lambda(0) \rightarrow \lambda(\tau)$. Applying Jensen's inequality to Eq. (2) gives $\langle W \rangle \geq \Delta F$, showing that Eq. (1) still holds merit but now in a statistical sense.

It is worth asking whether there are *optimal* protocols which meet the lower bound on the work W given by the equilibrium free energy difference ΔF , and, if they

exist, how they look like. For once this is useful because they can improve the estimation of said free energy difference via Eq. (2) [7]. Also, they could be an alternative or supplementary approach to large-deviation methods, e.g. optimizing the protocol instead of employing a more complicated large-deviation algorithm [8, 9]. The design of biological nanoscale machines is another aspect, where evolution might have designed them to be energy efficient and hence follow an optimized protocol.

With respect to optimal protocols, in past works mostly systems with few degrees of freedom, like single one-dimensional colloidal particles, have been considered so far [2–4, 10–12]. Some of the work includes numerical optimization, e.g., using threshold accepting [13] applied to a Brownian particle [3], or genetic algorithms [14, 15] applied to cyclic protocols for microscopic heat engines [11]. With respect to controlling systems, which exhibit many degrees of freedom and collective behavior, the Ising-model has also been studied, with temperature as an additional control parameter and the aim to invert the magnetization of a given system. Where notable contributions are restricted to the linear response regime [16], or are in the context of parametrized protocol ensembles [17].

With respect to the shape of optimal protocols, discontinuous jumps of the control-parameter value at the beginning and end are a reoccurring observation. Still, even moderate changes to simple systems can result in new and surprising features in the space of optimized protocols, e.g.: delta peaks for the underdamped langevin particle in a harmonic trap [4], regions with single or multiple jumps for a dipole potential [3], and the existence of phase transitions between optimal-work and optimal-work-fluctuations protocols [10].

In the present work the Higgs RNA-model [1] is studied with numerical simulations [18]. To the authors knowledge, it has not been investigated with regard to optimal protocols, despite its computational accessibility [19–21], see below, its many degrees of freedom, and its rich behavior like the occurrence of phase transitions [21–23] or finite-size glassy phases [24, 25].

Further, it is conceptually close to experimental setups

* peter.werner@uni-oldenburg.de

† a.hartmann@uni-oldenburg.de

of single DNA hairpin experiments that try to implement optimized protocols [26]. This makes the model, beyond its importance for molecular biology, an ideal playground to investigate various fundamental questions concerning optimized protocols, e.g.: How are specific system state trajectories affected? What role do phase transitions play when it comes to optimality of protocols? Are there general rules on how work distributions change, especially in the large-deviation regime? How do optimized protocols change with regard to the energy landscape, which is determined by the primary structure of the RNA molecule? Given the space and time constraints, this paper addresses only some of these questions but it is clear that the RNA model is useful also for further investigations beyond this proof of principle study.

The structure of this paper is as follows: First, the Higgs RNA-model is described, followed by the algorithms used to implement the work process as controlled by a given work protocol. Next, the parallel tempering scheme is described, used to find optimized protocols. In the main part, findings are presented, which include the shape of the optimized protocols, mean trajectories of system observables and resulting work distributions.

II. MODEL

The *primary structure* of a RNA molecule is given by a linear sequence $\mathcal{R} = (r_i)_{i=1,\dots,L}$ of L bases $r_i \in \{A, C, G, U\}$, where the four letters correspond to the bases Adenine, Cytosine, Guanine and Uracil. Two bases r_i, r_j at positions i and j (with $1 \leq i < j \leq L$) can pair to each other with energy $e(r_i, r_j) < 0$, where the set of all pairs (i, j) then forms the so called *secondary structure* \mathcal{S} . It has four constraints:

- (1) A base can pair to at most one other base.
- (2) Only *complementary* (Watson-Crick) A-U and C-G pairs are allowed.
- (3) *Pseudoknots* are excluded, i.e., two arbitrary pairs $(i, j), (i', j') \in \mathcal{S}$ with $i < i'$ must either fulfill $i < j < i' < j'$ or $i < i' < j' < j$.
- (4) There is a minimum distance $|j - i| > s$ between two paired bases (here $s = 2$).

For bases r, r' , the pairing energy is set to $e(r, r') = -1$ when r and r' are complementary and $e(r, r') = +\infty$ otherwise. To allow for manipulation of the system, the protocol $\lambda(t)$, which takes the role of an external force parameter, couples to the *free length* $n = n(\mathcal{S})$ of the secondary structure \mathcal{S} , yielding an additional energy of $-\lambda(t) \times n$. The free length $n(\mathcal{S})$ is defined as the number of bases with an sequence index that does not lie between those of any base-pair currently a part of the secondary

structure \mathcal{S} :

$$n(\mathcal{S}) = \sum_{i=1}^L c_i \quad (3)$$

$$c_i = \begin{cases} 0 & \text{if } \exists (j, k) \in \mathcal{S} : j < i < k \\ 1 & \text{else} \end{cases}$$

The total energy is finally given by the contributions from all base pairs and the external manipulation:

$$E(\mathcal{S}, \lambda) = \sum_{(i,j) \in \mathcal{S}} e(r_i, r_j) - n(\mathcal{S})\lambda, \quad (4)$$

where the explicit dependence on the primary structure is omitted. This model has been used previously in other statistical mechanics frameworks [9, 21] and is a strong simplification compared to those when describing real RNA. Dedicated software packages like ViennaRNA [27] exist that incorporate interactions of natural RNA more comprehensively. But using such a sophisticated model would add details related to RNA's biological function which is outside the scope of the more fundamental statistical-mechanics questions that are of interest here.

In the following, secondary structures in equilibrium are drawn from a canonical ensemble at temperature T , i.e., they occur with the Boltzmann probability $P(\mathcal{S}) \sim \exp(-E(\mathcal{S}, \lambda)/T)$. In equilibrium, typical RNA sequences exhibit an folding-unfolding transition at a sequence and slightly temperature-dependent critical value $\lambda_c(T)$.

III. ALGORITHMS

A. RNA work process

The work process is realized as a non-equilibrium Monte-Carlo simulation, where the duration τ of the process is proportional to the total number of MC-Sweeps n_{MC} , i.e. $\tau \sim n_{\text{MC}}$. One MC-step is the insertion or removal of a single base-pair in the secondary structure \mathcal{S} and one MC-sweep consists of $L/2$ MC-steps.

A major advantage, at this point, of the described RNA-model is that the equilibrium behaviors, i.e., the canonical partition function is calculable via dynamic programming in $\mathcal{O}(L^3)$. With this comes the ability to efficiently sample the initial equilibrium states following the Gibbs-Boltzmann distribution directly in $\mathcal{O}(L^2)$ [9, 19]. This allows to start every work process with a secondary structure sampled in equilibrium. For details on the sampling see appendix A.

Given a protocol $\lambda_j = \lambda(t_j)$ at discrete points in time $t_j = j\Delta\tau$ with $j = 0, \dots, n_\tau$, $\Delta\tau = \tau/n_\tau$, the work process then goes as displayed in Fig. 1.

Note that the work process allows for explicit incorporation of jumps at, e.g., the beginning and end of the protocol, since these are believed to be a generic feature of optimal protocols [2]. This was done in other

```

algorithm  $W[\lambda(t)]$ 
begin
  draw for  $\mathcal{R}$  an equilibrium structure  $\mathcal{S}$  at
  initial protocol value  $\lambda_0$  and RNA temperature  $T$ 
   $W = 0$ 
  for  $j = 1, \dots, n_\tau$ 
  begin
     $\Delta\lambda = \lambda_j - \lambda_{j-1}$ 
     $W = W - n(\mathcal{S})\Delta\lambda$ 
    perform  $L n_{MC}/(2n_\tau)$  MC-steps over  $\mathcal{S}$ 
  end
  return( $W$ )
end

```

FIG. 1. Algorithm to perform an unfolding process resulting in a work W .

numerical studies on the topic, too [10]. For comparison, also a naive linear protocols is studied with $\Delta\lambda = (\lambda_\tau - \lambda_0)/n_\tau = \text{const.}$ as presented below.

B. Optimization Algorithm

Following [3], the work protocol $\lambda(t)$ is discretized by $n = 42$ control points that are varied by the optimization scheme to approximate the optimal protocol. For a representation of the protocol at finer resolution these n points are interpolated linearly in between, except for the possible explicit jumps at start and end, to yield a total of $n_\tau = 200 + 2$ points, including the fixed start $\lambda_0 = 0$ and end which is chosen to be $\lambda_\tau = 2$.

The objective function of the optimization process for the protocol $\lambda(t)$ is the average work $\bar{W} = \frac{1}{N} \sum_{i=1}^N W_i$, determined by a finite number N of work process executions, yielding N work values W_i .

The optimization occurs in two stages. For both stages, Markov-chain Monte Carlo simulations with the Metropolis-Hasting algorithm are performed in the space of protocols. For any given protocol, exhibiting mean work \bar{W} , trial protocols are constructed by randomly selecting one of the n variable protocol points λ_j and changing it by a random amount according to $\lambda_j \leftarrow |\lambda_j + 2\varepsilon\delta\lambda| \pmod{2\lambda_\tau}$, which are periodic boundary conditions for λ_j that could assist to find certain features, especially delta peaks, when sampling the protocol space. Where $\varepsilon \in (0, 1]$ is a uniformly distributed random number and $\delta\lambda$ is a magnitude chosen as described below. The final optimization result is not expected to change when alternatively using more commonly employed reflective boundary conditions, i.e., moves are rejected when moving outside the allowed interval.

For the trial protocol, N work processes are performed and a corresponding mean work \bar{W}' is obtained. The trial protocols are accepted for the Markov chain with an Metropolis probability $\min\{1, \exp[-(\bar{W}' - \bar{W})/\theta]\}$, which corresponds to a Boltzmann distribution of the

TABLE I. Overview of investigated primary structure sequences \mathcal{R}

<i>hairpin</i>	$(AC)^{10}(GU)^{10} = ACAC\dots GUGU$
<i>continuous</i>	$(ACGU)^{10}$
<i>asymmetric</i>	$(AC)^5(GU)^5(ACGU)^5$

mean work values for a given artificial “temperature” θ .

For the first stage, the parallel tempering method [28] at 100 artificial temperatures θ_i with logistic spacing is used, i.e., $\theta_i = \theta_0(\delta\theta)^i$, ranging from $\theta_0 = 8 \cdot 10^{-4}$ to $\theta_{99} = 50$. The control parameter $\delta\lambda$ is chosen for each value θ_i such that the empirical acceptance rate is around 0.5 for this move, respectively. Here, $N = 1000$ independent work processes are generated to calculate the mean work of every protocol. The tempering is run until all replicas could visit a sufficient fraction of all temperature sites.

The second stage is given by an annealing simulation at $\theta = 0$ with an increased number $N = 10^5$ of work processes, starting from the best protocol found in the previous stage. For $\delta\lambda$, the same value is used as it was at θ_0 in the first stage.

One caveat with this approach, in order to work, is to fix the random numbers used to generate the work processes, i.e. resetting the random number generator to the same initial state before starting sampling, which is conceptually similar to what is done in [3] with the noise history. This is necessary, because two independent evaluations of the mean work, performed for the same work protocol, must yield exactly the same value of \bar{W} .

The numerical optimization does not necessarily yield an exact optimal protocol due to the finite work sample size and the random nature of the algorithm itself, i.e. maybe the optimum gets never selected within protocol space. But even close to optimal protocols, as discussed in [17], will likely poses the distinct features, e.g. jumps, that are responsible for achieving optimality.

IV. RESULTS

Three primary structure sequences of length $L = 40$ are investigated (see Tab. I). Note that calculation of partitions functions and sampling can be achieved for much larger system length L , but here we optimize over the protocols, such that every single optimization step consists of a full simulation according to the algorithm shown in Fig. 1. Still, the system investigated here consist of several interacting particles, in contrast to most work in the literature.

The first considered sequence can fold into a perfect *hairpin* secondary structure at low temperature T and small force λ . The second sequence is constructed by repeating the four bases over and over again, i.e., it is a *continuous* sequence. The third sequence represents a combination of the *hairpin* and *continuous* sequence, which is called *asymmetric* here. Sequences like these,

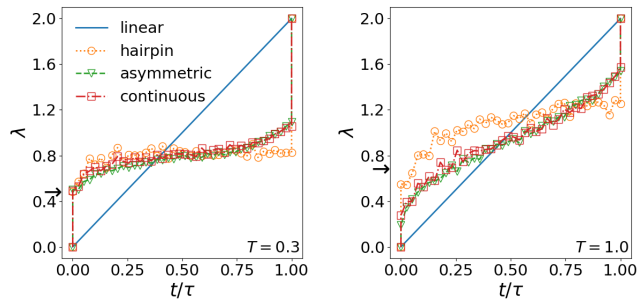


FIG. 2. Optimized protocols λ as a function of time t , which display distinct jumps at the beginning and end. The linear protocol is also shown for reference. The arrow on the vertical axis indicates the critical value λ_c of the folding-unfolding transition. Left: $T = 0.3$. Right: $T = 1.0$.

which all can fold into secondary structures with one or more hairpins, are relevant due to their abundant occurrence in nature and treatment in previous studies [29–36]. The work simulations are performed at two temperatures $T \in \{0.3, 1.0\}$ which are representative for the sequences being in or close to the ground state, or where several relevant secondary structures contribute, respectively. The three considered sequences exhibit folding-unfolding transitions at critical values near $\lambda_c = 0.5$ for $T = 0.3$ and near $\lambda_c = 0.7$ for $T = 1$.

A. Optimized Protocols

Fig. 2 shows the optimized protocols as a function of time and the naive linear protocol for comparison. The rugged structure likely stems from the finite number of work processes, which contribute to the average work \overline{W} , and the optimization scheme itself, identifying only one of the exponentially many close to optimal protocols [17]. Here, the most striking feature is the existence of distinct jumps at the beginning and end, present for all sequences at both temperatures. The jump heights at beginning and end are always different from each other and are lower at the higher temperature $T = 1.0$ compared to $T = 0.3$. Further, the *continuous* and *asymmetric* sequences have rather similar optimal protocols, despite the later one also having partially a primary structure like the *hairpin* sequence. Jumps are also observed for simpler systems like brownian-particles [2–4], giving further indication that they are indeed a generic feature of optimized protocols as was already speculated in Ref. [2]. Fitting a 5th order polynomial to the protocol to obtain a smoothed version does not change the qualitative result presented below, i.e. the work distributions in Fig. 5 are effectively unaltered by using the smoothed protocols.

A more refined analysis is obtained here by recording secondary structure trajectories, while the system is subject to the corresponding protocol. This is used to measure the mean free length. The force λ as a function

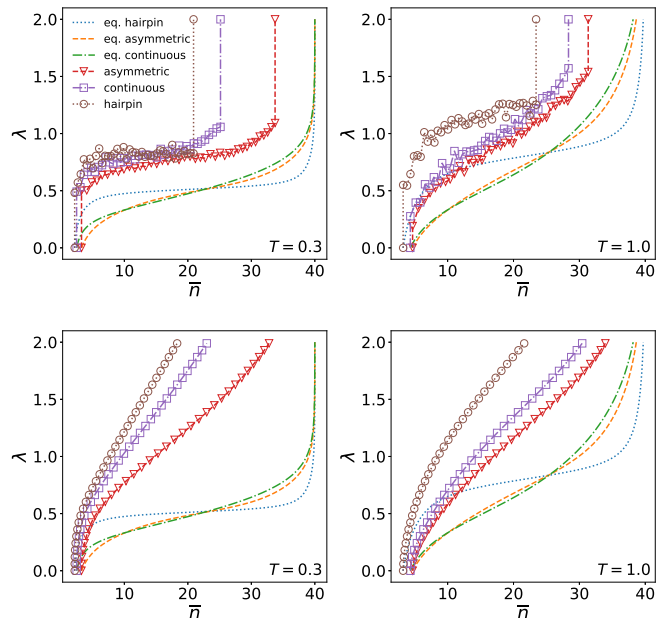


FIG. 3. Protocols λ as a function of mean free length \bar{n} . The equilibrium curves are also shown for reference. Top: Optimized protocols. The initial jumps are close to the equilibrium unfolding transition point. Bottom: Linear protocols for comparison. Left: $T = 0.3$. Right: $T = 1.0$.

of mean free length \bar{n} , i.e. $\bar{n}(\lambda)$ with switched axes, is depicted in Fig. 3 together with the equilibrium curves, which are obtained by utilizing the partition function. Here, it becomes apparent how optimality is achieved: The first jump at the beginning is into the regime of the force unfolding equilibrium phase transition. Staying close to the transition point in the flowing, the free length of the system increases due to interaction with the heat bath, where energy is taken from. This allows the second jump at the end to happen with on average higher free length and therefore resulting in a lower overall work performed. On the other hand, the vicinity to the critical equilibrium protocol value may appear surprising, since one expects the system dynamics to slow down, which generates more lag to equilibrium and therefore increases dissipation [37]. Indeed, opposite behavior, i.e. the avoidance of critical points, has been observed for example in the reorientation of spins in an Ising-system [16, 17], where temperature was an additional protocol parameter that allows the protocol to circumvent the system's critical line. Another major difference is that for the Ising system the process is between two opposite ordered states, while here the system is driven from folded to unfolded structures. Also, the protocol in the present study can not avoid the force unfolding transition anyway. As a result, varying the protocol only slightly while crossing the critical point, gives the system more time to equilibrate or staying close to equilibrium, i.e., reducing the lag between the system current and equilibrium distribution. For this reason, the optimized protocols also tend to ap-

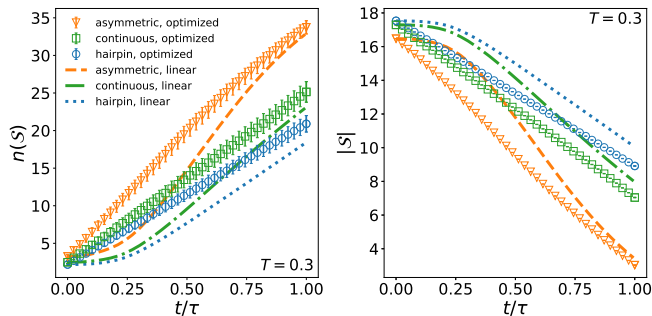


FIG. 4. Mean system observables as a function of time t for $T = 0.3$. The trajectories for the optimized protocols have an almost linear behavior. Left: Mean free length \bar{n} . Right: Mean number of paired bases $|\mathcal{S}|$.

proximate the equilibrium curves (Fig. 3 top), especially when compared to the naive linear protocol behaviour (Fig. 3 bottom).

B. Trajectories

How does the optimal protocol change the system trajectories compared to a naive linear protocol? In Fig. 4 the mean free length \bar{n} and the mean number of paired bases $|\mathcal{S}|$ is plotted as a function of time for both protocols and $T = 0.3$. The $T = 1.0$ case looks similar. Remarkably, the behavior for the optimized protocols is in all cases almost linear, while the linear protocol results in more sigmoidal trajectories. The free length for optimized protocol is higher in the beginning than for the linear protocol, indicating that the unfolding of the secondary structure is quicker. In the same train of thought, the number of base pairs decreases for the optimized protocol faster than for the naive linear protocol.

C. Work Distributions

The resulting work distributions for the linear and optimized protocols are depicted in Fig. 5. The general trend is, as expected since the optimized protocols aim at minimizing the work, that the probability is shifted to lower values of W . For $T = 1.0$, the peak of the distributions for the optimized protocols, compared to the linear ones, generally move only slightly but increase in height, while the tails towards high work values lose statistical weight. In case of $T = 0.3$, not only the peak moves but the distribution shape undergoes significant change. The *hairpin* sequence work distribution shows an prominent oscillatory peak structure as well as the right distribution tail for the continues sequence. This structure is a result of the discrete free length values, the slow system dynamics and that the highest contribution to the final work comes from the initial and final jump, since the protocol changes only slightly in between them.

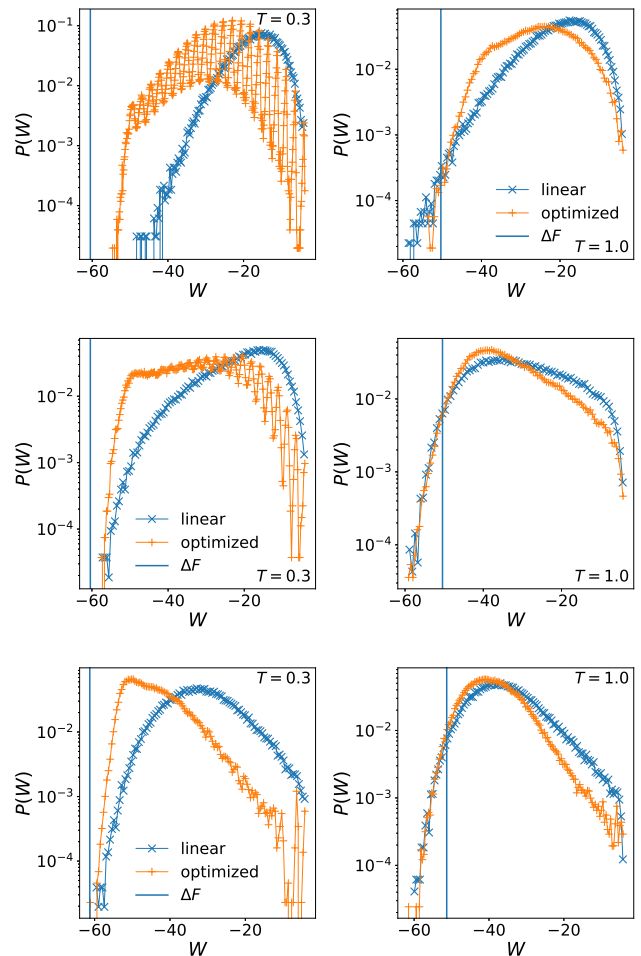


FIG. 5. Work distributions for the linear and optimized protocols. Top: *Hairpin* sequence. Middle: *Continuous* sequence. Bottom: *Asymmetric* sequence. 10^5 work processes are used to estimate the histograms, except for the optimized protocol at $T = 0.3$ for the *hairpin* sequence, where 4×10^5 processes are generated. Lines are a guide to the eye only.

Work distributions with such erratic behavior have been observed before, e.g. for the simple model system in [5], and are therefore not limited or specific to optimized protocols.

Also shown are the exact free energy differences ΔF , directly obtained from the partition function. Even a qualitative inspection of the distributions reveals that there is no substantial improvement compared to the linear protocol case, judging from the intersection of $P(W)$ with ΔF , which is relevant for its estimation when using, e.g., Crooks theorem [5]. This underlines the importance of large-deviation algorithms [8, 9] for such purposes, and that mere protocol optimization is not equivalent or even superior.

For further investigation of the work distributions, a sampling of the initial secondary structures with fixed free length values $n(\mathcal{S}_0)$ was performed. The subsequence

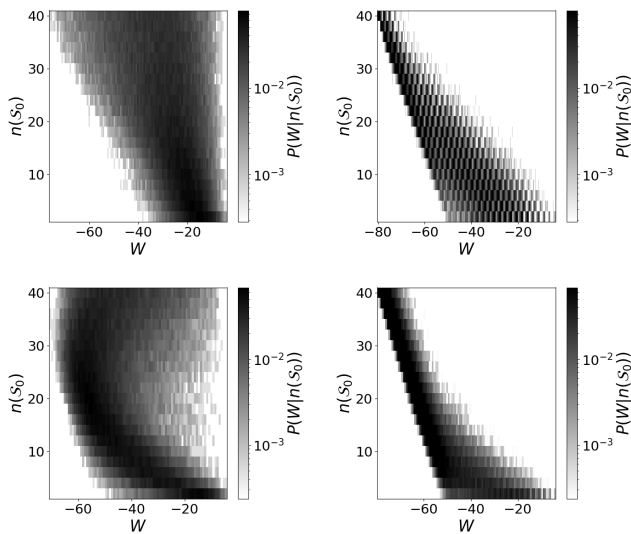


FIG. 6. Shade coded work distributions conditioned to the initial free length $n(S_0)$ at $T = 0.3$. A darker shade corresponds to a higher probability. For each initial free length 5500 work processes are sampled. Left: Linear protocol. Right: Optimized protocol. Top: *Hairpin* sequence. Bottom: *Continuous* sequence.

work processes yielded distributions $P(W|n(S_0))$ conditioned to said initial free length. The results are displayed in Fig. 6). In comparison to the linear protocol, the optimized protocols especially affect the work of processes with rare high initial free lengths. Since the optimized protocol immediately increases the force λ , the resulting structures are less likely to fold towards a more probable state with lower free length during the work process. This ultimately leads to consistently lower work values for such cases. For the linear protocol the opposite is true: The low initial force allows the structure to fold before being unfolded again, resulting in a wide spread of work values. For the *continuous* sequence and linear protocol, the weight is more concentrated at smaller values of W as compared to the *hairpin* sequence, most clear for values near $n(S_0) \approx 26$. It is due to secondary structures predominantly consisting of multiple small hairpins next to each other at the beginning of the work process. Under an external force, these unfold all individually, i.e. the free length increases more rapidly than for a single hairpin, because there are more base pairs that would increase the free length when removed. This leads on average to an overall lower work compared to the *hairpin* sequence.

V. DISCUSSION

Numerically optimized protocols for simple *hairpin* sequences were presented for the Higgs-RNA model, which is a model exhibiting many interacting degrees of freedom. These optimized protocols show similar distinct

jumps as observed before for systems with only one degree of freedom. As discussed, the optimized protocols have a connection to the unfolding equilibrium phase transition and allow the system to better approximate equilibrium behavior in order to reduce dissipation. The corresponding work distributions, although shifted to lower work values, revealed qualitatively that a priori no substantial improvement to free-energy estimations can be expected from mere protocol optimization. Investigating work distributions conditioned to the initial free length of the process has shown that especially very unlikely starting values are affected by optimized protocols. Due to this last aspect, the employment of a large-deviation algorithm in combination with optimized protocols, to sample the work distributions in the relevant rare event regime, could be a promising perspective. Also it would be interesting to see whether the results obtained here can be found for work processes performed for other complex interacting systems.

ACKNOWLEDGMENTS

This work used the Scientific Compute Cluster at GWDG, the joint data center of Max Planck Society for the Advancement of Science (MPG) and University of Göttingen.

Appendix A: Equilibrium Sampling of Secondary Structures with Fixed Free Length

For a system given by Eq. (4) with force parameter $\lambda = 0$ and any primary structure \mathcal{R} , the canonical partition function $Z_{i,j}$ can be calculated for all possible subsequences r_i, \dots, r_j ($i \leq j$) via

$$Z_{i,j} = Z_{i,j-1} + \sum_{k=i}^{j-s-1} Z_{i,k-1} e^{-\beta e(r_k, r_j)} Z_{k+1, j-1}, \quad (\text{A1})$$

using appropriate starting conditions. In a similar fashion, the partition function $Q_{1,j,n}$ at fixed free length n for all subsequences r_1, \dots, r_j ($1 \leq j$) is obtained using

$$Q_{1,j,n} = Q_{1,j-1,n-1} + \sum_{k=n-1}^{j-s-1} Q_{1,k-1,n-2} e^{-\beta e(r_k, r_j)} Z_{k+1, j-1}, \quad (\text{A2})$$

again with compatible starting values. All of this can be done using *dynamical programming* in $O(L^3)$ runtime [19]. By dividing Eq. (A2) by $Q_{1,j,n}$, the individual terms can be identified as pairing probabilities. First, the probability of base j being unpaired:

$$p_{j,n}^u = \frac{Q_{1,j-1,n-1}}{Q_{1,j,n}}. \quad (\text{A3})$$

The remaining terms are the probabilities that base j is paired to any base k with $n-1 \leq k \leq j-s-1$:

$$p_{j,k,n}^p = \frac{Q_{1,k-1,n-2} e^{-\beta e(r_k, r_j)} Z_{k+1, j-1}}{Q_{1,j,n}}. \quad (\text{A4})$$

The sampling is then done via the recursive scheme described in [9] and roughly goes as follows: For a given subsequence from base i to j with so far no pair, begin-

ning with $i = 1$ and $j = L$, base j is randomly paired to another base k in the subsequence using the corresponding pairing probabilities. If base j remains unpaired, the scheme is continued by setting $j' = j - 1$. Should base j be paired to base k , the recursive procedure is independently continued for the two created subsequence from $i' = i$ to $j' = k - 1$ and $i' = k + 1$ to $j' = j - 1$.

-
- [1] P. G. Higgs, *Physical Review Letters* **76** (1996), 10.1103/PhysRevLett.76.704.
- [2] T. Schmieidl and U. Seifert, *Phys. Rev. Lett.* **98**, 108301 (2007).
- [3] H. Then and A. Engel, *Phys. Rev. E* **77**, 041105 (2008).
- [4] A. Gomez-Marin, T. Schmieidl, and U. Seifert, *The Journal of Chemical Physics* **129**, 024114 (2008), <https://doi.org/10.1063/1.2948948>.
- [5] G. E. Crooks, *Phys. Rev. E* **60**, 2721 (1999).
- [6] G. E. Crooks, **90**, 1481.
- [7] P. Geiger and C. Dellago, *Phys. Rev. E* **81**, 021127 (2010).
- [8] A. K. Hartmann, **89**, 10.1103/PhysRevE.89.052103.
- [9] P. Werner and A. K. Hartmann, *Phys. Rev. E* **104**, 034407 (2021).
- [10] A. P. Solon and J. M. Horowitz, *Phys. Rev. Lett.* **120**, 180605 (2018).
- [11] R. Xu, *Journal of Statistical Physics* **184**, 29 (2021).
- [12] S. Blaber, M. D. Louwerse, and D. A. Sivak, *Phys. Rev. E* **104**, L022101 (2021).
- [13] G. Dueck and T. Scheuer, *J. Comput. Phys.* **90**, 161 (1990).
- [14] D. E. Goldberg, *Genetic Algorithms in Search, Optimization and Machine Learning* (Addison-Wesley, Reading (MA), 1989).
- [15] Z. Michalewicz, *Genetic Algorithms + Data Structures = Evolution Programs* (Springer, Heidelberg, 1994).
- [16] G. M. Rotskoff and G. E. Crooks, *Phys. Rev. E* **92**, 060102 (2015).
- [17] T. R. Gingrich, G. M. Rotskoff, G. E. Crooks, and P. L. Geissler, *Proceedings of the National Academy of Sciences* **113**, 10263 (2016), <https://www.pnas.org/doi/pdf/10.1073/pnas.1606273113>.
- [18] A. K. Hartmann, *Big Practical Guide to Computer Simulations* (World Scientific, Singapore, 2015).
- [19] R. Nussinov, G. Pieczenik, J. R. Griggs, and D. J. Kleitman, *SIAM Journal on Applied Mathematics* **35**, 68 (1978).
- [20] R. Nussinov and A. B. Jacobson, *Proc. Natl. Acad. Sci. USA* **77**, 6309 (1980).
- [21] M. Müller, F. Krzakala, and M. Mézard, *Eur. Phys. J. E* **9**, 67.
- [22] R. Bundschuh and T. Hwa, *Phys. Rev. E* **65**, 031903 (2002).
- [23] B. Burghardt and A. K. Hartmann, *Phys. Rev. E* **71**, 021913 (2005).
- [24] A. Pagnani, G. Parisi, and F. Ricci-Tersenghi, *Phys. Rev. Lett.* **84**, 2026 (2000), [arXiv:cond-mat/9907125](https://arxiv.org/abs/cond-mat/9907125).
- [25] A. K. Hartmann, *Phys. Rev. Lett.* **86**, 1382 (2001).
- [26] S. Tafoya, S. J. Large, S. Liu, C. Bustamante, and D. A. Sivak, *Proc Natl Acad Sci U S A* **116**, 5920 (2019).
- [27] R. Lorenz, S. Bernhart, C. Höner zu Siederdisen, H. Tafer, C. Flamm, P. Stadler, and I. Hofacker, *Algorithms for molecular biology : AMB* **6**, 26 (2011).
- [28] D. J. Earl and M. W. Deem, *Phys. Chem. Chem. Phys.* **7**, 3910 (2005).
- [29] R. Bundschuh and T. Hwa, *Phys. Rev. Lett.* **83**, 1479 (1999).
- [30] U. Gerland, R. Bundschuh, and T. Hwa, *Biophysical Journal* **81**, 1324 (2001).
- [31] M. Faber and S. Klumpp, *Phys. Rev. E* **88**, 052701 (2013).
- [32] F. Liu, H. Tong, and Z. can Ou-Yang, *Biophysical Journal* **90**, 1895 (2006).
- [33] F. Liu and Z. can Ou-Yang, *Biophysical Journal* **88**, 76 (2005).
- [34] J. Liphardt, S. Dumont, S. B. Smith, I. Tinoco, and C. Bustamante, *Science* **296**, 1832 (2002), <https://www.science.org/doi/pdf/10.1126/science.1071152>.
- [35] D. Collin, F. Ritort, C. Jarzynski, S. B. Smith, I. Tinoco, and C. Bustamante, *Nature* **437**, 231 (2005).
- [36] J. Liphardt, B. Onoa, S. B. Smith, I. Tinoco, and C. Bustamante, *Science* **292**, 733 (2001), <https://www.science.org/doi/pdf/10.1126/science.1058498>.
- [37] S. Vaikuntanathan and C. Jarzynski, *EPL (Europhysics Letters)* **87**, 60005 (2009).